

Supporting Information for

## **DNA Origami Voltage Sensors for Transmembrane Potentials with Single-Molecule Sensitivity**

Sarah E. Ochmann<sup>†</sup>, Himanshu Joshi<sup>‡</sup>, Ece Büber<sup>†</sup>, Henri G. Franquelim<sup>§</sup>, Pierre Stegemann<sup>⊥</sup>, Barbara Saccà<sup>⊥</sup>, Ulrich F. Keyser<sup>||</sup>, Aleksei Aksimentiev<sup>‡</sup>, Philip Tinnefeld<sup>\*,†</sup>

<sup>†</sup>Department of Chemistry and Center for NanoScience, Ludwig-Maximilians-Universität München, 81377 München, Germany

<sup>‡</sup>Department of Physics and Beckman Institute for Advanced Science and Technology, University of Illinois, Urbana, Illinois 61820, United States

<sup>§</sup>Max Planck Institute of Biochemistry, 82152 Planegg, Germany

<sup>⊥</sup>Centre for Medical Biotechnology (ZMB) and Centre for Nano Integration Duisburg-Essen (CENIDE), University of Duisburg-Essen, Universitätsstraße 2, 45117 Essen, Germany

<sup>||</sup>Cavendish Laboratory, Department of Physics, University of Cambridge, JJ Thomson Avenue, Cambridge, CB3 0HE, United Kingdom

\*Corresponding author: Philip Tinnefeld: [philip.tinnefeld@cup.uni-muenchen.de](mailto:philip.tinnefeld@cup.uni-muenchen.de)

## Material and Methods

### *Experimental part*

#### Chemicals

If not declared differently, all chemicals were purchased from Merck KGaA.

#### DNA origami folding

A rectangular DNA origami<sup>1</sup> was used which is based on a 7249 nt long scaffold derived from the M13mp18 bacteriophage. It was designed in the software CaDNA<sup>2</sup> and carried several modifications as indicated in Figure S1. All staple strand sequences are given in Table S1 together with the name of the company from which it was purchased.

The origami structures were folded in buffer containing 10 mM Tris, 1 mM EDTA and 12.5 mM MgCl<sub>2</sub> by mixing 10 nM of the scaffold with 100 nM of unmodified and 300 nM of modified oligonucleotides. The solution was heated to 70°C for 3 min and then cooled down in 1°C-steps remaining 1 min at each temperature in a thermocycler (primus 25, peqlab). During the folding process, the biotin modified oligonucleotides, the binding site containing an ATTO532 dye and three cholesterol strands on a ssDNA leash were incorporated. By PEG precipitation, the folded structures were purified from excess staple strands where the sample was mixed in a 1:1 ratio with a buffer containing 12% PEG-8000 (w/v), 10 mM Tris, 1 mM EDTA, 500 mM NaCl and 12 mM MgCl<sub>2</sub> at pH 7.5 and centrifuged for 30 min at 16 krcf and 4°C. The supernatant was discarded and the pellet dissolved in the buffer used for folding. This step was repeated 4 times. In order to label the DNA origami with seven more cholesterol and the voltage-sensing unit, it was incubated over night at room temperature with 5x excess of the oligonucleotides named above per binding site, before another PEG precipitation for purification was examined. The samples were stored at 4°C until usage.

#### Liposome preparation

To produce Large Unilamellar Vesicles (LUVs), lipid films were created. Therefore 1,2-dioleoyl-sn-glycero-3-phosphocholine (DOPC, Avanti Polar Lipids, INC.) was dissolved at a concentration of 25 mg/mL in chloroform and 1 mmol was added to a glass vial, dried under a nitrogen stream and for another 4 h under vacuum in a desiccator. These lipid films were stored at -20°C until further usage. To create LUVs, the lipid films were dissolved in LUV buffer containing 5 mM Tris, 1 mM EDTA, 0.5 mM Trolox and either 150 mM KCl or 149 mM NaCl and 1 mM KCl at pH 7 (potassium or sodium LUV buffer, respectively) resulting in a lipid concentration of 2.5 mM. After seven freeze-and-thaw cycles using liquid nitrogen and a 80°C water bath, the solution was extruded with a LiposoFast Basic extruder (Avestin, INC.) using Nucleopore PC membranes with a pore size of 100 nm (Whatman, Cytiva Ltd.).

#### Preparation of microscope slides

Nunc Lab-Tek II Chambered Slides (Thermo Fisher Scientific Inc.) were cleaned with 1 M KOH for 4 h at room temperature. After washing with 1xPBS buffer, the slides were passivated over night at 4°C with 0.5 mg/mL PLL(20)-g[3.5]- PEG(2)/PEG(3.4)- biotin(50%) (PLL-PEG-biotin, SuSoS AG) in 1xPBS. After washing with 1xPBS, 0.25 mg/mL NeutrAvidin (Thermo Fisher Scientific Inc.) in 1xPBS was added for 20 min and washed off with 1xPBS and the slides were ready to use.

## TIRF microscope

A homebuilt Total Internal Reflection (TIRF) microscope based on an Olympus IX71 inverted microscope was used for the single-molecule Fluorescence Resonance Energy Transfer (smFRET) measurements. The beams of a green laser (Sapphire 532 nm, 100 mW, Coherent) and a red laser (iBeam Smart 640 nm, 150 mW, Toptica Photonics) were altered using an acousto-optical tunable filter (AOTF, PCAOM-VIS, Crystal Technology) at a frequency of 10 Hz. The power of the green laser was set to 30 mW and of the red laser to 80 mW. The light was focused on the sample with an oil-immersion objective (APO N 60XO/1.49 NA TIRF, Olympus). The emission light was separated from the excitation light by a dual line beamsplitter and further separated into 2 emission channels with an Optosplit III (Cairn Research) equipped with a dichroic beam splitter (640 DCXR, Chroma Technology). The green emission was spectrally filtered with a bandpass filter (BrightLine HC 582/75, Semrock) and the red emission with a longpass filter (647 nm RazorEdge, Semrock), before being focused on a back-illuminated sCMOS camera (KURO 1200B sCMOS, Princeton Instruments) in a dual-view configuration. The LightField software (Princeton Instruments) was used to acquire videos with a length of each min. 300 frames.

## Sample preparation and imaging

To obtain DNA origami-liposome complexes, the DNA origami were incubated with the liposomes with a 100x excess of the liposomes over the origami for 2 h at room temperature in the respective LUV buffer (potassium or sodium). Then the structures were immobilized in Lab-Tek chambers at a concentration of 30 pM via biotin-neutravidin interaction and imaged on the homebuilt TIRF microscope described above. The LUV buffer matching the ion composition inside of the liposome was used. These measurements represent the control samples, before in each of these samples an electrical transmembrane potential  $\Delta\Psi$  was built up.

To then create the electrical transmembrane potential  $\Delta\Psi$ , first the buffer surrounding the origami-liposome complexes was exchanged with respect to the desired potential. To determine the ionic gradient required, the Nernst equation

$$\Delta\Psi = \frac{RT}{Fz} \ln \left( \frac{c_{in}^{K^+}}{c_{out}^{K^+}} \right) \quad (1)$$

with R as the universal gas constant, T as the temperature, F as the Faraday constant, z as the charge number and  $c_{in}^{K^+}$  or  $c_{out}^{K^+}$  as the  $K^+$  concentration inside or outside of the liposome, respectively, was used. Table S2 shows the concentrations of KCl and NaCl used to create the different electrical potentials tested. Secondly, 7.5 nmol of valinomycin was added which locates into the hydrophobic core of the lipid bilayer, complexes potassium ions and shuttles them through the lipid membrane while the Chloride counter ions remain. Thereby an electrical transmembrane potential  $\Delta\Psi$  is built up.<sup>3</sup> After an incubation of 10 min with the valinomycin, the samples were imaged again on the homebuilt TIRF microscope. For the liposome-free sample, the DNA origami were immobilized without prior LUV incubation and imaged in buffer containing 10 mM Tris, 1 mM EDTA, 0.5 mM Trolox, 149 mM NaCl and 1 mM KCl at pH 7.

## Data analysis

For the data analysis, the software iSMS<sup>4</sup> running on Matlab was used. The split channels of green and red emission were superimposed and from the videos an intensity-time transient was derived for each single spot. These transients were then carefully revised to separate single DNA origami structures showing FRET from multimers or origami not containing both fluorophores. In the three channels of donor excitation-donor emission  $D_{exc}-D_{em}$ , donor excitation-acceptor emission  $D_{exc}-A_{em}$  and acceptor excitation-acceptor emission  $A_{exc}-A_{em}$  it was checked for a correlation typical for single-molecule FRET pairs. If there was a clear correlation between the different channels – e.g. an intensity increase in the  $D_{exc}-D_{em}$  channel while a decrease in the  $D_{exc}-A_{em}$  channel is observed upon a simultaneous drop in the  $A_{exc}-A_{em}$  channel – the transient was picked and the period selected over which the mean *Proximity Ratio*  $PR$  was calculated as

$$PR = \frac{I_{DA}}{I_{DD} + I_{DA}} \quad (2)$$

with  $I_{DA}$  as the intensity from the  $D_{exc}-A_{em}$  channel and  $I_{DD}$  as the intensity from the  $D_{exc}-D_{em}$  channel. The data derived this way was further plotted against its frequency and a Gauss fit was used to determine the mean  $PR$  and its standard error for each sample.

The change  $\Delta PR$  shown in Figure 3 and 4 was calculated as

$$\Delta PR = PR - PR_{before} \quad (3)$$

with  $PR$  as the value determined for the respective sample with the transmembrane potential  $\Delta\Psi = x$  mV and  $PR_{before}$  as the value derived before the addition of valinomycin. The respective standard error  $\sigma_{\Delta PR}$  resulted from a Gaussian error propagation as

$$\sigma_{\Delta PR} = \sqrt{\left(\left|\frac{\partial \Delta PR}{\partial PR}\right| \cdot \sigma_{PR}\right)^2 + \left(\left|\frac{\partial \Delta PR}{\partial PR_{before}}\right| \cdot \sigma_{PR_{before}}\right)^2} \quad (4)$$

## Valinomycin bulk test

To proof that valinomycin creates electrical transmembrane potential  $\Delta\Psi$  in liposomes that have a potassium gradient between the in- and outside, a bulk assay was performed using the voltage-sensitive fluorophore 3,3'-Dipropylthiadicarbocyanine Iodide (DiSC<sub>3</sub>(5), Thermo Fisher Inc.), liposomes and the spectrofluorometer FS5 (Edinburgh Instruments). The DiSC<sub>3</sub>(5) dye is cationic and accumulates on hyperpolarized lipid membranes where its fluorescence is reduced due to contact quenching. Hence, the fluorescence intensity depends on the electrical potential of the lipid membrane.

High precision cell cuvettes (Ultra-Micro Cell 105.252-QS, Hellma analytics) were passivated with a 1 mg/mL BSA solution (Sigma Aldrich) in 1xPBS buffer to decrease unspecific binding. 100  $\mu$ L of LUVs with a lipid concentration of 200  $\mu$ M were added. The buffer inside the liposome for each sample tested contained 5 mM Tris, 1 mM EDTA, 0.5 mM Trolox and 150 mM KCl at pH7. The buffer in which the LUVs were diluted to the respective concentration was either the same or instead of the 150 mM KCl contained 149 mM NaCl and 1 mM KCl. The respective buffer combination for each sample is depicted in Figure S4.

The DiSC<sub>3</sub>(5) dye was added to the liposome containing cuvette resulting at a final concentration of 1  $\mu$ M and an addition of 1% (v/v) DMSO to the solution. After an incubation of 10 min, the sample was placed in the spectrofluorometer and the acquisition started ( $\lambda_{\text{ex}}$ =666 nm, bandwidth<sub>ex</sub>=1 nm,  $\lambda_{\text{em}}$ =691 nm, bandwidth<sub>em</sub>=5 nm, 1 point/s). Once the fluorescence intensity was stable, valinomycin was added resulting in a final concentration of 500 nM and another 0.25% (v/v) DMSO, so the final DMSO concentration in the cuvette was 1.25% (v/v). Then the effect of valinomycin was followed by tracking of the fluorescence intensity. For the samples testing the influence of the buffer on the fluorescence intensity, instead of the valinomycin solution, only the respective buffer outside of the liposome was added together with the same overall DMSO concentration of 1.25% (v/v).

To first neglect an interference between the DiSC<sub>3</sub>(5) and valinomycin, the ionophore was added to the free dye (Figure S4a). After the addition, the fluorescence baseline is lower than before, but no further effect is observed. The intensity drop can be affiliated to unspecific binding of the dye to the pipette tip; the overall dye concentration is slightly reduced and as a consequence, the fluorescence signal, too. This underlines the importance to not mix the following samples by multiple pipetting to reduce the effect.

Next, the effect of adding a solution to the liposome-dye mixture was investigated. Therefore the respective buffer with DMSO was added to liposomes with inside and outside potassium buffer (Figure S4b) and with inside potassium and outside sodium buffer (Figure S4c) liposomes. After the addition, for both samples an equilibration towards a higher intensity is observed which is related to a homogeneous distribution after Brownian motion in the field of view. As for the free dye, the baseline is slightly reduced though due to unspecific dye sticking to the pipette tip. Anyhow, no specific intensity decrease is observed. Next, the effect of valinomycin to the liposome-dye mixture was tested when there is no ion gradient to the outside (Figure S4d) and as previously, no change is observed which means that no polarization at the lipid membrane is induced.

Lastly, as in the single molecule experiments, valinomycin was added to a sample with potassium carrying liposomes in sodium buffer with DiSC<sub>3</sub>(5) (Figure S4e). Unlike in the samples before, after the valinomycin addition the intensity baseline is not only lower, but also an equilibration towards a lower intensity is observed. This different behavior clearly proofs that a transmembrane potential  $\Delta\Psi$  is built up and the cationic voltage-sensing dye is attracted to the hyperpolarized membrane where its accumulation leads to contact quenching and hence, a reduced overall intensity.

## *Simulation part*

### General simulation protocols

All MD simulations were performed using program NAMD<sup>5</sup>, a 2 fs integration time step, 2-2-6 multiple time stepping, periodic boundary conditions and particle mesh Ewald (PME) method over a 1 Å resolution grid to calculate the long range electrostatic interaction.<sup>6</sup> The Nose-Hoover Langevin piston<sup>7</sup> and Langevin thermostat were used to maintain the constant pressure and temperature in the system. An 8-10-12 Å cutoff scheme was used to calculate van der Waals and short-range electrostatic forces. SETTLE algorithm<sup>8</sup> was applied to keep water molecules rigid whereas RATTLE algorithm<sup>9</sup> constrained all other covalent bonds involving hydrogen atoms. CHARMM36 force field parameters described the bonded and non-bonded interactions among the atoms of DNA<sup>10</sup>, lipid<sup>11</sup>, water and ions.<sup>12</sup> Magnesium

ions were modeled as magnesium hexahydrates ( $\text{Mg}[\text{H}_2\text{O}]_6^{2+}$ ).<sup>13</sup> Corrections to non-bonded interactions potentials were applied to improve description of ion-DNA, ion-ion, and DNA-lipid interactions.<sup>14</sup> CHARMM General Force Field (CGenFF)<sup>15</sup> were used to describe the interaction parameters for the dye molecules. The coordinates of the system were saved at an interval of 20 ps. The visualization, analysis and post-processing of the simulation trajectories were performed using VMD<sup>16</sup> and CPPTRAJ.<sup>17</sup>

## Initial models of lipid bilayer membrane and dye conjugated DNA

Starting with the caDNAno design of DNA origami plate along with the modified strands for anchoring and voltage sensing (Figure S1 and Table S1), we performed coarse-grained MD simulation using mrDNA resulting in the movie S3.<sup>18</sup> The final configuration of the origami plate at the end of the coarse-grained simulation was converted to an all-atom model. In order to obtain the nanoscale structure and dynamics of the dye molecules conjugated to the DNA fragment, we selected the 22 base-pair long DNA strand containing the dye molecules in experimental design. The topology and parameters file for the ATTO647N and ATTO532 dye molecules covalently conjugated using  $\text{C}_{12}+\text{C}_6$  linker molecules to DNA were obtained using the CHARMM General Force Field (CGenFF) webserver.<sup>19</sup> We used a custom psfgen script in VMD to covalently connect the dye molecules to DNA according to the chemical sketch shown in Figure S2.  $\text{Mg}^{2+}$ -hexahydrates were placed near the DNA to neutralize its electrical charge of the DNA backbone.

We simulated two analogs of the dye conjugated DNA, one in an aqueous environment and another anchored in the lipid bilayer membrane leading to the data shown in Figure S3 and the Movies S1 and S2. To create the system in aqueous environment, the dye conjugated DNA molecule was solvated with TIP3P water molecules<sup>20</sup> using the Solvate plugin of VMD.<sup>16</sup> Potassium and chloride ions were added to produce 150 mM concentration of KCl in solution using the Autoionize plugin of VMD. Thus, assembled system measured  $8 \times 8 \times 15 \text{ nm}^3$  and contained approximately 80,000 atoms. To create the membrane-anchored DNA system, we placed the dye conjugated DNA molecule in a pre-equilibrated patch of 1,2-dioleoyl-sn-glycero-3-phosphocholine (DOPC) lipid bilayer membrane such that the ATTO647N and  $\text{C}_{12}$  spacer connecting it to the DNA span in the upper leaflet of the membrane. The lipid patch was generated using the CHARMM-GUI membrane builder<sup>21</sup> and pre-equilibrated for approximately 200 ns. Finally, we solvated the system with TIP3P water molecules<sup>20</sup> and added ions to produce a 150 mM concentration of KCl. Thus, the membrane-anchored system measured  $10 \times 10 \times 15 \text{ nm}^3$  and contained approximately 130,000 atoms.

The assembled systems were subjected to energy minimization using the conjugate gradient method to remove the steric clashes between the solute and solvent. Following that, we equilibrated each system for 20 ns while harmonically restraining the phosphorus (P) atoms of DNA using a spring constant of  $1 \text{ kcal mol}^{-1} \text{ \AA}^{-2}$ . Subsequently, we equilibrated the systems for additional 40 ns while maintaining the hydrogen bonds between the complementary base-pairs of DNA using the extrabond utility of NAMD. Finally, we removed all the restraints (except two P atoms of each DNA strand connecting the DNA to the origami plate) and performed approximately 1  $\mu\text{s}$  long production simulations of systems using a constant number of atoms (N), pressure ( $P = 1 \text{ bar}$ ) and temperature ( $T = 300 \text{ K}$ ), the NPT ensemble. Two sets of simulations were carried for each design to improve sampling of the conformational space.

The simulation results presented in Figure S3b for the system without a membrane unravel a very close and stable state of the two fluorophores in the pink trajectory after  $\sim 0.75 \mu\text{s}$ . Inspecting Movie S1, melting of the dsDNA can be observed which leads to the dyes touching each other. Direct contact between dyes commonly yields complex photophysics with different intensity levels<sup>22,23</sup> that is not observed in our experiments. We therefore assign the DNA melting and the direct dye-dye contact to a force field artefact in the simulation which has been previously observed for CHARMM36 force fields as used in our system.<sup>24</sup> Therefore, for Figure 1f only data is included before the artefact is observed eliminating the prominent peak around  $10 \text{ \AA}$  visible in Figure S3c. Also, for both the system with and without a lipid membrane, the first  $0.2 \mu\text{s}$  of the simulation are excluded as this is approximately the time the system needs to equilibrate.

## Double-membrane systems

To mimic the voltage bias created by a difference in the ionic concentration from inside to outside of a lipid vesicle in our simulations, we created a double membrane system having two identical patches of DOPC lipid bilayer membrane kept at a distance of  $9 \text{ nm}$  away from each other (distance between the center of the membranes) along the bilayer normal. We solvated the double DOPC membrane system using TIP3P water molecules<sup>20</sup> and added ions to produce  $150 \text{ mM}$  concentration of KCl. Thus, assembled double membrane system measured  $11 \times 11 \times 20 \text{ nm}^3$  and contains  $218,400$  atoms.

The assembled system was subjected to energy minimization using the conjugate gradient method to remove the steric clashes between the solute and solvent. Following that, we equilibrated the double membrane system for  $230 \text{ ns}$  using the NPT ensemble. Towards the end of the equilibration, the distance between the center of the mass (CoM) of the individual bilayer along the bilayer normal stabilizes close to  $8.8 \text{ nm}$ . Averaging the dimensions of the simulation box from the last  $20 \text{ ns}$  of the NPT equilibration, we next performed simulation of the double membrane system in NVT ensemble. We created two other double membrane system named as  $1 \text{ K}^+$  and  $-1 \text{ K}^+$ , by shuffling one potassium ion from the inside chamber (the bulk water region around the center of the simulation box) to the outside chamber (the bulk water region at both ends of the simulation box) and vice-versa. Thus, we generated three double-membrane systems:  $0 \text{ K}^+$  system having exactly same number of potassium ions inside and outside,  $1 \text{ K}^+$  system having two more potassium ions inside as compared to outside and  $-1 \text{ K}^+$  system having two fewer potassium ions inside as compared to the outside which is equivalent to a transmembrane potential of  $\Delta\Psi = \pm 180 \text{ mV}$  for this system's geometry. Finally, all systems were simulated using NVT ensemble with the exact same box dimension for approximately  $300 \text{ ns}$ . The data is presented in Figure S7.

## Free energy calculations of dsDNA binding to double-membrane systems

Starting from a pre-equilibrated conformation of  $21$  base pair long dsDNA kept over a  $10 \times 7.1 \text{ nm}^2$  patch of DPhPE lipid membrane from our earlier study,<sup>25</sup> we created a DNA double membrane system by replicating another copy of the simulation cell along the bilayer normal. The DNA fragment is effectively infinite along its helical axis as both of the strands are connected to themselves across the periodic boundary (along the  $y$ -axis). We removed dsDNA and neutralizing counterions ( $42$  potassium ions) from the outer chamber, which left us with the desired system having dsDNA only in the inner chamber of the double membrane and  $150 \text{ mM}$  concentration of KCl in solution (Figure S7a). Thus, assembled DNA double membrane system was measured  $10 \times 7.1 \times 25 \text{ nm}^3$  and contains  $181,628$  atoms.

Both, the inner and outer chamber of this double membrane-DNA system are charge neutralized and we refer to this system as 0 K<sup>+</sup>.

Next, we created two other systems, 4 K<sup>+</sup> and -4 K<sup>+</sup> by shuffling 4 potassium ions from the outer chamber to the inner chamber and *vice-versa* inducing a potential of  $\Delta\Psi=\pm 1.3$  V, a high enough value to observe statistically significant differences in the interactions between the DNA and the membrane without causing membrane electroporation. Thus, we have three systems with the same number of atoms but different potassium ions in inner and outer chambers. In 0 K<sup>+</sup>, both the chambers are electrically charge-neutral, 4 K<sup>+</sup> system has 8e<sup>+</sup> charge in inner chamber as compared to the outer chamber and -4 K<sup>+</sup> system has 8 e<sup>+</sup> charge in the outer chamber as compared to the inner one due the shuffling of the potassium ions.

Twenty-one copies of each system were created by moving the CoM of dsDNA from 13 to 33 Å along the z-axis, the region shown using an arrow in Figure S7a. Note that Z =0 corresponds to the center of the simulation cell. Since the CoM of the upper membrane lies at z = 63 Å, the distance of the CoM of dsDNA and upper membrane varies from 50 to 13 Å in respective copies of the simulation system. Replica exchange umbrella sampling simulations<sup>26</sup> were performed using the 1 Å sampling window for the distance between the CoM of dsDNA's and the upper membrane along the z-axis. A harmonic potential with the spring constant of 2.5 kcal/mol/ Å<sup>2</sup> was used to maintain the distance between dsDNA and the membrane in each window along the z-axis using colvars module<sup>27</sup> of NAMD. Each replica was run for approximately 120 ns. Weighted histogram analysis method (WHAM)<sup>28</sup> was used to subtract the effect of the harmonic potential and obtain the PMF profile. The first 5 ns of the simulation trajectories were excluded from the WHAM analysis.



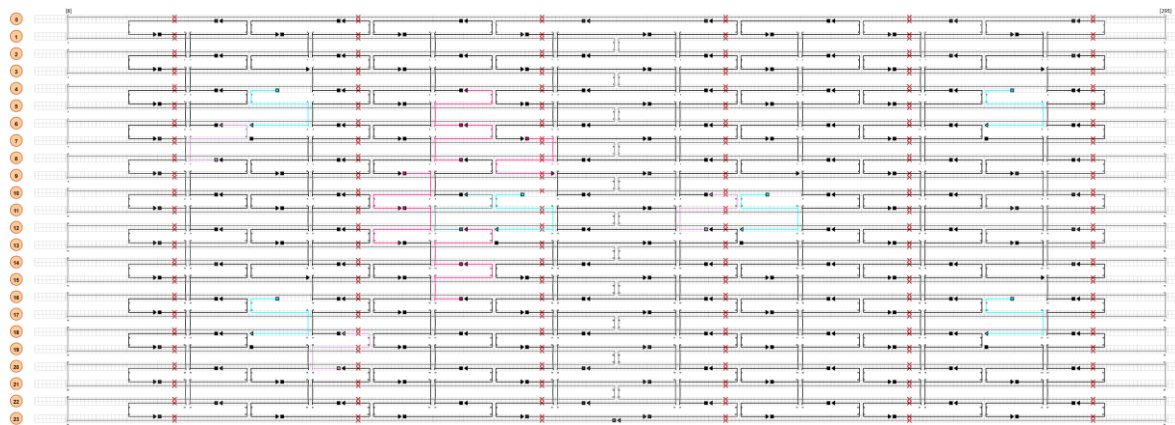


**Figure S1. Illustration of DNA origami design in CaDNAno<sup>2</sup>.** The number of helices is shown in orange on the left and the nucleotide position described in the grid starting at position [8] and ending at position [295] (top). The scaffold strand is presented in dark grey, the unmodified staple strands in black, the biotinylated strands in blue carrying the modification on the 5' end, in light pink strands with cholesterol on the 3' end of a ssDNA spacer, in dark pink cholesterol attached via dsDNA on the 5' end and in cyan the voltage-sensing unit on the 5' end. The sequences of the strands and more details can be found in Table S1.

**Table S1. DNA oligonucleotides used as staple strands for the DNA origami voltage sensor.** The staple stands are listed with the 5' position x[y] with x as the helix number and y as the nucleotide number as described in Figure S1, the DNA sequence from the 5' to the 3' end, further modifications in the comment section and the company purchased from. Nucleotides in bold are not incorporated into the DNA origami, but protrude from the structure. For 12[111], either a or b are incorporated.

5' position	Sequence (5' to 3' end)	Comments	Company
/	TATGAGTGTACACGATTGTTAAAA[SpC12][ATTO647N]	Voltage sensor C <sub>12</sub> +C <sub>6</sub> , binds to 12[111]a strand [ATTO647N]: modification on amino-C6 linker [SpC12]: C <sub>12</sub> spacer	biomers.net GmbH
/	[ATTO647N]AAATAACAATCGTGTACACTCATA	Voltage sensor C <sub>12</sub> , binds to 12[111]b strand [ATTO647N]: modification on amino-C <sub>12</sub> linker	biomers.net GmbH
12[111] a	TAACA[ATTO532]ATCGTGTACACTCATATAAATCATATAACCTGTTTAGCTAACCTTTAA	Binding site for voltage sensor C <sub>12</sub> +C <sub>6</sub> [ATTO532]: modification on amino-C <sub>6</sub> -dT linker	Eurofins Genomics GmbH
12[111] b	TAAATCATATAACCTGTTTAGCTAACCTTTAATATGAGTGTACACGAT[ATTO532]TGTTA	Binding site for voltage sensor C <sub>12</sub> [ATTO532]: modification on amino-C <sub>6</sub> -dT linker	Eurofins Genomics GmbH
20[79]	TTCCAGTCGTAATCATGGTCATAAAAGGGGAAAAAAAAA [Chol]	[Chol]: Cholesterol-TEG modification	Integrated DNA Technologies, Inc.
8[47]	ATCCCCCTATACCACATTCAACTAGAAAAATCAAAAAAAAAA [Chol]	[Chol]: Cholesterol-TEG modification	Integrated DNA Technologies, Inc.
12[175]	TTTTATTTAAGCAAATCAGATATTTTTGTAAAAAAAAA [Chol]	[Chol]: Cholesterol-TEG modification	Integrated DNA Technologies, Inc.
/	GTGATGTAGGTGGTAGAGGA [Chol]	Cholesterol strand, binds to multiple binding sites depicted below [Chol]: Cholesterol-TEG modification	Integrated DNA Technologies, Inc.
11[96]	TCCTCTACCACCTACATCACAATGGTCAACAGGCAAGGCAAAGAGTAATGTG	Cholesterol binding site	Eurofins Genomics GmbH
14[111]	TCCTCTACCACCTACATCACGAGGGTAGGATTCAAAGGGTGAGACATCCAA	Cholesterol binding site	Eurofins Genomics GmbH
6[111]	TCCTCTACCACCTACATCACATTACCTTTGAATAAGGCTTGC CCAATCCGC	Cholesterol binding site	Eurofins Genomics GmbH

5' position	Sequence (5' to 3' end)	Comments	Company
7[128]	TCCTCTACCACCTACATCACAGACGACAAAGAAGTTTGGCC ATAATTTCGAGCTTCAA	Cholesterol binding site	Eurofins Genomics GmbH
8[111]	TCCTCTACCACCTACATCACAATAGTAAACACTATCATAACC CTCATTGTGA	Cholesterol binding site	Eurofins Genomics GmbH
16[111]	TCCTCTACCACCTACATCACTGTAGCCATTAAAATTTCGCATT AAATGCCGGA	Cholesterol binding site	Eurofins Genomics GmbH
9[96]	TCCTCTACCACCTACATCACCGAAAGACTTTGATAAGAGGT CATATTTCCGA	Cholesterol binding site	Eurofins Genomics GmbH
21[64]	GCCCTTCAGAGTCCACTATTAAAGGGTGCCGT		Eurofins Genomics GmbH
1[160]	TTAGGATTGGCTGAGACTCCTCAATAACCGAT		Eurofins Genomics GmbH
15[96]	ATATTTTGGCTTTCATCAACATTATCCAGCCA		Eurofins Genomics GmbH
22[271]	CAGAAGATTAGATAATACATTGTGCGACAA		Eurofins Genomics GmbH
5[128]	AACACCAAATTTCAACTTTAATCGTTTACC		Eurofins Genomics GmbH
20[47]	TTAATGAACTAGAGGATCCCCGGGGGTAACG		Eurofins Genomics GmbH
18[79]	GATGTGCTTCAGGAAGATCGCACAATGTGA		Eurofins Genomics GmbH
12[207]	GTACCGCAATTCTAAGAACGCGAGTATTATTT		Eurofins Genomics GmbH
4[271]	AAATCACCTTCAGTAAGCGTCAGTAATAA		Eurofins Genomics GmbH
22[207]	AGCCAGCAATTGAGGAAGGTTATCATCATTTT		Eurofins Genomics GmbH
8[207]	AAGGAAACATAAAGGTGGCAACATTATCACCG		Eurofins Genomics GmbH
15[128]	TAAATCAAATAATTTCGCGTCTCGGAAACC		Eurofins Genomics GmbH
6[271]	ACCGATTGTCGGCATTTTCGGTCATAATCA		Eurofins Genomics GmbH
0[79]	ACAACTTTCAACAGTTTCAGCGGATGTATCGG		Eurofins Genomics GmbH
11[224]	GCGAACCTCCAAGAACGGGTATGACAATAA		Eurofins Genomics GmbH
8[239]	AAGTAAGCAGACACCACGGAATAATATTGACG		Eurofins Genomics GmbH
19[96]	CTGTGTGATTGCGTTGCGCTCACTAGAGTTGC		Eurofins Genomics GmbH
15[224]	CCTAAATCAAATCATAGGTCTAAACAGTA		Eurofins Genomics GmbH
1[192]	GCGGATAACCTATTATTCTGAAACAGACGATT		Eurofins Genomics GmbH
5[160]	GCAAGGCCTCACCAGTAGCCATGGGCTTGA		Eurofins Genomics GmbH
12[239]	CTTATCATTCGCGACTTGCGGGAGCCTAATTT		Eurofins Genomics GmbH
2[111]	AAGGCCGCTGATACCGATAGTTGCGACGTTAG		Eurofins Genomics GmbH
19[248]	CGTAAACAGAAATAAAAAATCCTTTGCCGAAAGATTAGA		Eurofins Genomics GmbH
0[111]	TAAATGAATTTTCTGTATGGGATTAATTTCTT		Eurofins Genomics GmbH
5[32]	CATCAAGTAAACGAACTAACGAGTTGAGA		Eurofins Genomics GmbH
20[207]	GCGGAACATCTGAATAATGGAAGGTACAAAAT		Eurofins Genomics GmbH
12[143]	TTCTACTACGCGAGCTGAAAAGGTTACCGCGC		Eurofins Genomics GmbH
8[143]	CTTTTGCAGATAAAAACAAAATAAAGACTCC		Eurofins Genomics GmbH
2[143]	ATATTCGGAACCATCGCCACGCAGAGAAGGA		Eurofins Genomics GmbH
21[224]	CTTTAGGGCCTGCAACAGTGCCAATACGTG		Eurofins Genomics GmbH
14[239]	AGTATAAAGTTCAGCTAATGCAGATGTCTTTC		Eurofins Genomics GmbH
20[111]	CACATTAAAATTGTTATCCGCTCATGCGGGCC		Eurofins Genomics GmbH
3[128]	AGCGCGATGATAAATTGTGTCGTGACGAGA		Eurofins Genomics GmbH
17[128]	AGGCAAAGGGAAGGGCGATCGGCAATTCCA		Eurofins Genomics GmbH
17[160]	AGAAAACAAAGAAGATGATGAAACAGGCTGCG		Eurofins Genomics GmbH
2[207]	TTTCGGAAGTGCCGTCGAGAGGGTGAGTTTCG		Eurofins Genomics GmbH
22[79]	TGGAACAACCGCTGGCCCTGAGGCCGCT		Eurofins Genomics GmbH
10[47]	CTGTAGCTTGACTATTATAGTCAGTTCATTGA		Eurofins Genomics GmbH
16[207]	ACCTTTTTATTTTAGTTAATTTTCATAGGGCTT		Eurofins Genomics GmbH

5' position	Sequence (5' to 3' end)	Comments	Company
9[224]	AAAGTCACAAAATAAACAGCCAGCGTTTAA		Eurofins Genomics GmbH
19[224]	CTACCATAGTTTGAGTAACATTTAAATAT		Eurofins Genomics GmbH
3[96]	ACACTCATCCATGTTACTTAGCCGAAAGCTGC		Eurofins Genomics GmbH
18[239]	CCTGATTGCAATATATGTGAGTGATCAATAGT		Eurofins Genomics GmbH
10[239]	GCCAGTTAGAGGGTAATTGAGCGCTTTAAGAA		Eurofins Genomics GmbH
3[32]	AATACGTTTGAAAGAGGACAGACTGACCTT		Eurofins Genomics GmbH
1[128]	TGACAACTCGCTGAGGCTTGCAATTATACCA		Eurofins Genomics GmbH
16[47]	ACAAACGGAAAAGCCCCAAAACACTGGAGCA		Eurofins Genomics GmbH
14[175]	CATGTAATAGAAATAAAAGTACCAAGCCGT		Eurofins Genomics GmbH
17[192]	CATTGAAGGCGAATTATTCATTTTGTTTGG		Eurofins Genomics GmbH
19[56]	TACCGAGCTCGAATTCGGGAAACCTGTCGTGCAGCTGATT		Eurofins Genomics GmbH
6[111]	ATTACCTTTGAATAAGGCTTGCCCAAATCCGC		Eurofins Genomics GmbH
23[64]	AAAGCACTAAATCGGAACCCTAATCCAGTT		Eurofins Genomics GmbH
16[175]	TATAACTAACAAAGAACGCGAGAACGCCAA		Eurofins Genomics GmbH
7[56]	ATGCAGATACATAACGGGAATCGTCATAAATAAGCAAAG		Eurofins Genomics GmbH
3[224]	TTAAAGCCAGAGCCGCCACCTCGACAGAA		Eurofins Genomics GmbH
12[47]	TAAATCGGGATTCCCAATTCTGCGATATAATG		Eurofins Genomics GmbH
3[160]	TTGACAGGCCACCACCAGAGCCGCGATTGTGA		Eurofins Genomics GmbH
14[143]	CAACCGTTTCAAATCACCATCAATTCGAGCCA		Eurofins Genomics GmbH
6[79]	TTATACCACCAAATCAACGTAACGAACGAG		Eurofins Genomics GmbH
4[239]	GCCTCCCTCAGAATGGAAAGCGCAGTAACAGT		Eurofins Genomics GmbH
7[248]	GTTTATTTTGTACAACTTTACCGAAGCCCTTTAATATCA		Eurofins Genomics GmbH
1[32]	AGGCTCCAGAGGCTTTGAGGACACGGGTAA		Eurofins Genomics GmbH
0[207]	TCACCAGTACAACTACAACGCCTAGTACCAG		Eurofins Genomics GmbH
4[143]	TCATCGCCAACAAAGTACAACGGACGCCAGCA		Eurofins Genomics GmbH
16[271]	CTTAGATTTAAGGCGTTAAATAAAGCCTGT		Eurofins Genomics GmbH
13[96]	TAGGTAACTATTTTGTAGAGATCAAACGTTA		Eurofins Genomics GmbH
21[192]	TGAAAGGAGCAAATGAAAAATCTAGAGATAGA		Eurofins Genomics GmbH
5[224]	TCAAGTTTCATTAAAGGTGAATATAAAAGA		Eurofins Genomics GmbH
14[111]	GAGGGTAGGATTCAAAGGGTGAGACATCCAA		Eurofins Genomics GmbH
8[79]	AATACTGCCCCAAAAGGAATTACGTGGCTCA		Eurofins Genomics GmbH
11[160]	CCAATAGCTCATCGTAGGAATCATGGCATCAA		Eurofins Genomics GmbH
4[111]	GACCTGCTCTTTGACCCCCAGCGAGGGAGTTA		Eurofins Genomics GmbH
2[175]	TATTAAGAAGCGGGTTTTGCTCGTAGCAT		Eurofins Genomics GmbH
13[184]	GACAAAAGGTAAAGTAATCGCCATTTTAACAAAACTTTT		Eurofins Genomics GmbH
1[96]	AAACAGCTTTTTTGCGGGATCGTCAACACTAAA		Eurofins Genomics GmbH
23[192]	ACCCTTCTGACCTGAAAGCGTAAGACGTGAG		Eurofins Genomics GmbH
15[32]	TAATCAGCGGATTGACCGTAATCGTAACCG		Eurofins Genomics GmbH
18[175]	CTGAGCAAAAATTAATTACATTTTGGGTTA		Eurofins Genomics GmbH
6[175]	CAGCAAAAGGAAACGTACCAATGAGCCGC		Eurofins Genomics GmbH
18[47]	CCAGGGTTGCCAGTTTGAGGGGACCCGTGGGA		Eurofins Genomics GmbH
6[143]	GATGGTTTGAACGAGTAGTAAATTTACCATTA		Eurofins Genomics GmbH
8[175]	ATACCCAACAGTATGTTAGCAAATTAGAGC		Eurofins Genomics GmbH

5' position	Sequence (5' to 3' end)	Comments	Company
17[96]	GCTTCCGATTACGCCAGCTGGCGGCTGTTTC		Eurofins Genomics GmbH
12[79]	AAATTAAGTTGACCATTAGATACTTTTGCG		Eurofins Genomics GmbH
8[271]	AATAGCTATCAATAGAAAATTCAACATTCA		Eurofins Genomics GmbH
15[192]	TCAAATATAACCTCCGGCTTAGGTAACAATTT		Eurofins Genomics GmbH
21[96]	AGCAAGCGTAGGGTTGAGTGTGTAGGGAGCC		Eurofins Genomics GmbH
20[239]	ATTTTAAATCAAAATTATTTGCACGGATTCTG		Eurofins Genomics GmbH
7[224]	AACGCAAAGATAGCCGAACAAACCCTGAAC		Eurofins Genomics GmbH
20[79]	TTCCAGTCGTAATCATGGTCATAAAAGGGG		Eurofins Genomics GmbH
22[239]	TTAACACCAGCACTAACAACTAATCGTTATTA		Eurofins Genomics GmbH
18[111]	TCTTCGCTGCACCGCTTCTGGTGCGGCCTTCC		Eurofins Genomics GmbH
17[32]	TGCATCTTCCCAGTCACGACGGCCTGCAG		Eurofins Genomics GmbH
4[175]	CACCAGAAAGGTTGAGGCAGGTCATGAAAG		Eurofins Genomics GmbH
13[120]	AAAGGCCGAGACAGCTAGCTGATAAATTAATTTTGT		Eurofins Genomics GmbH
10[175]	TTAACGTCTAACATAAAAAACAGTAACGGA		Eurofins Genomics GmbH
21[256]	GCCGTCAAAAAACAGAGGTGAGGCCTATTAGT		Eurofins Genomics GmbH
4[47]	GACCACTAATGCCACTACGAAGGGGGTAGCA		Eurofins Genomics GmbH
6[239]	GAAATTATTGCCTTTAGCGTCAGACCGGAACC		Eurofins Genomics GmbH
18[271]	CTTTTACAAAATCGTCGCTATTAGCGATAG		Eurofins Genomics GmbH
14[79]	GCTATCAGAAATGCAATGCCTGAATTAGCA		Eurofins Genomics GmbH
2[47]	ACGGCTACAAAAGGAGCCTTTAATGTGAGAAT		Eurofins Genomics GmbH
21[128]	GCGAAAAATCCCTTATAAATCAAGCCGGCG		Eurofins Genomics GmbH
22[175]	ACCTTGCTTGGTCAGTTGGCAAAGAGCGGA		Eurofins Genomics GmbH
8[47]	ATCCCCCTATACCACATTCAACTAGAAAAATC		Eurofins Genomics GmbH
1[64]	TTTATCAGGACAGCATCGGAACGACCAACCTAAAACGA		Eurofins Genomics GmbH
17[224]	CATAAATCTTTGAATACCAAGTGTTAGAAC		Eurofins Genomics GmbH
16[143]	GCCATCAAGCTCATTTTTTAACCACAAATCCA		Eurofins Genomics GmbH
4[207]	CCACCCTCTATTCACAAACAAATACCTGCCTA		Eurofins Genomics GmbH
2[79]	CAGCGAACTTGCTTTTCGAGGTGTTGCTAA		Eurofins Genomics GmbH
19[128]	CACAACAGGTGCCTAATGAGTGCCAGCAG		Eurofins Genomics GmbH
19[192]	ATTATACTAAGAAACCACCAGAAGTCAACAGT		Eurofins Genomics GmbH
16[239]	GAATTTATTTAATGGTTTGAAATATTCTTACC		Eurofins Genomics GmbH
22[111]	GCCCCGAGAGTCCACGCTGGTTTGAGCTAACT		Eurofins Genomics GmbH
6[207]	TCACCGACGCACCGTAATCAGTAGCAGAACCG		Eurofins Genomics GmbH
13[224]	ACAACATGCCAACGCTCAACAGTCTTCTGA		Eurofins Genomics GmbH
20[175]	ATTATCATTCATATAATCCTGACAATTAC		Eurofins Genomics GmbH
18[207]	CGCGCAGATTACCTTTTTTAATGGGAGAGACT		Eurofins Genomics GmbH
12[175]	TTTTATTTAAGCAAATCAGATATTTTTTGT		Eurofins Genomics GmbH
10[207]	ATCCAATGAGAATTAACGAACAGTTACCAG		Eurofins Genomics GmbH
14[207]	AATTGAGAATTCTGTCCAGACGACTAAACCAA		Eurofins Genomics GmbH
13[64]	TATATTTTGTCAATGCTGAGAGTGGAAGATTGTATAAGC		Eurofins Genomics GmbH
7[128]	AGACGACAAAGAAGTTTGGCATAATTCGAGCTTCAA		Eurofins Genomics GmbH
7[160]	TTATTACGAAGAACTGGCATGATTGCGAGAGG		Eurofins Genomics GmbH
23[96]	CCCGATTTAGAGCTTGACGGGGAAAAAGAATA		Eurofins Genomics GmbH

5' position	Sequence (5' to 3' end)	Comments	Company
3[192]	GGCCTTGAAGAGCCACCACCTCAGAAACCAT		Eurofins Genomics GmbH
4[79]	GCGCAGACAAGAGGCAAAAGAATCCCTCAG		Eurofins Genomics GmbH
15[160]	ATCGCAAGTATGTAAATGCTGATGATAGGAAC		Eurofins Genomics GmbH
5[96]	TCATTGATGCGATTTTAAGAACAGGCATAG		Eurofins Genomics GmbH
18[143]	CAACTGTTGCGCCATTGCGCATTCAAACATCA		Eurofins Genomics GmbH
20[271]	CTCGTATTAGAAATTGCGTAGATACAGTAC		Eurofins Genomics GmbH
1[256]	CAGGAGGTGGGGTCAGTGCCTTGAGTCTCTGAATTTACCG		Eurofins Genomics GmbH
13[160]	GTAATAAGTTAGGCAGAGGCATTATGATATT		Eurofins Genomics GmbH
1[224]	GTATAGCAAACAGTTAATGCCCAATCCTCA		Eurofins Genomics GmbH
5[192]	CGATAGCATTGAGCCATTTGGAACGTAGAAA		Eurofins Genomics GmbH
7[192]	ATACATACCGAGGAAACGCAATAAGAAGCGCATTAGACGG		Eurofins Genomics GmbH
10[111]	TTGCTCCTTTCAAATATCGCGTTTGAGGGGGT		Eurofins Genomics GmbH
13[256]	GTTTATCAATATGCGTTATACAAACCGACCGTGTGATAAA		Eurofins Genomics GmbH
6[47]	TACGTTAAAGTAATCTTGACAAGAACCGAACT		Eurofins Genomics GmbH
16[79]	GCGAGTAAAAATATTTAAATTGTTACAAAAG		Eurofins Genomics GmbH
23[256]	CTTTAATGCGCGAACTGATAGCCCCACCAG		Eurofins Genomics GmbH
23[224]	GCACAGACAATATTTTTGAATGGGGTCAGTA		Eurofins Genomics GmbH
10[127]	TAGAGAGTTATTTTCATTTGGGGATAGTAGTAGCATT		Eurofins Genomics GmbH
4[63]	ATAAGGGAACCGGATATTCATTACGTCAGGACGTTGGGAA		Eurofins Genomics GmbH
16[63]	CGGATTCTGACGACAGTATCGGCCGCAAGCGATTAAAGTT		Eurofins Genomics GmbH
10[191]	GAAACGATAGAAGGCTTATCCGGTCTCATCGAGAACAAGC		Eurofins Genomics GmbH
16[255]	GAGAAGAGATAACCTTGCTTCTGTTCCGGAGAAACAATAA		Eurofins Genomics GmbH
4[255]	AGCCACCACTGTAGCGCGTTTCAAGGGAGGGAAGGTAAA		Eurofins Genomics GmbH
10[79]	GATGGCTTATCAAAAAGATTAAGAGCGTCC		Eurofins Genomics GmbH
0[47]	AGAAAGGAACAATAAAGGAATTCAAAAAAA		Eurofins Genomics GmbH
10[271]	ACGCTAACCCACAAGAATTGAAAATAGC		Eurofins Genomics GmbH
2[271]	GTTTTAACTTAGTACCGCCACCCAGAGCCA		Eurofins Genomics GmbH
14[271]	TTAGTATCACAATAGATAAGTCCACGAGCA		Eurofins Genomics GmbH
9[160]	AGAGAGAAAAAATGAAAATAGCAAGCAAACCT		Eurofins Genomics GmbH
12[271]	TGTAGAAATCAAGATTAGTTGCTCTTACCA		Eurofins Genomics GmbH
23[160]	TAAAAGGGACATTCTGGCCAACAAAGCATC		Eurofins Genomics GmbH
21[160]	TCAATATCGAACCTCAAATATCAATTCGAAA		Eurofins Genomics GmbH
19[160]	GCAATTCACATATTCCTGATTATCAAAGTGTA		Eurofins Genomics GmbH
10[143]	CCAACAGGAGCGAACCAGACCGAGCCTTTAC		Eurofins Genomics GmbH
23[32]	CAAATCAAGTTTTTTGGGGTCGAAACGTGGA		Eurofins Genomics GmbH
22[143]	TCGGCAAATCCTGTTTGATGGTGGACCTCAA		Eurofins Genomics GmbH
0[175]	TCCACAGACAGCCCTCATAGTTAGCGTAACGA		Eurofins Genomics GmbH
0[143]	TCTAAAGTTTTGTCGCTTTCCAGCCGACAA		Eurofins Genomics GmbH
20[143]	AAGCCTGGTACGAGCCGGAAGCATAGATGATG		Eurofins Genomics GmbH
2[239]	GCCCGTATCCGAATAGGTGTATCAGCCCAAT		Eurofins Genomics GmbH
7[32]	TTTAGGACAAATGCTTTAAACAATCAGGTC		Eurofins Genomics GmbH
23[128]	AACGTGGCGAGAAAGGAAGGAAACAGTAA		Eurofins Genomics GmbH
21[32]	TTTTCACTCAAAGGGCGAAAAACCATCACC		Eurofins Genomics GmbH

5' position	Sequence (5' to 3' end)	Comments	Company
14[47]	AACAAGAGGGATAAAAAATTTTAGCATAAAGC		Eurofins Genomics GmbH
13[32]	AACGCAAAATCGATGAACGGTACCGTTGA		Eurofins Genomics GmbH
0[271]	CCACCCTCATTTTCAGGGATAGCAACCGTACT		Eurofins Genomics GmbH
9[256]	GAGAGATAGAGCGTCTTCCAGAGGTTTTGAA		Eurofins Genomics GmbH
11[256]	GCCTTAAACCAATCAATAATCGGCACGCGCCT		Eurofins Genomics GmbH
0[239]	AGGAACCCATGTACCGTAACACTTGATATAA		Eurofins Genomics GmbH
9[32]	TTTACCCCAACATGTTTTAAATTTCCATAT		Eurofins Genomics GmbH
11[32]	AACAGTTTTGTACCAAAAACATTTTATTTT		Eurofins Genomics GmbH
22[47]	CTCCAACGCAGTGAGACGGGCAACCAGCTGCA		Eurofins Genomics GmbH
19[32]	GTCGACTTCGGCCAACGCGCGGGGTTTTTC		Eurofins Genomics GmbH
12[111]	TAAATCATATAACCTGTTTAGCTAACCTTTAA		Eurofins Genomics GmbH
7[96]	TAAGAGCAAATGTTTAGACTGGATAGGAAGCC		Eurofins Genomics GmbH
8[111]	AATAGTAAACACTATCATAACCTCATTGTGA		Eurofins Genomics GmbH
16[111]	TGTAGCCATTAAAATTCGCATTAAATGCCGGA		Eurofins Genomics GmbH
9[96]	CGAAAGACTTTGATAAGAGGTCATATTCGCA		Eurofins Genomics GmbH
11[64]	GATTTAGTCAATAAAGCCTCAGAGAACCCTCA		Eurofins Genomics GmbH
9[64]	CGGATTGCAGAGCTTAATTGCTGAAACGAGTA		Eurofins Genomics GmbH
11[96]	AATGGTCAACAGGCAAGGCAAAGAGTAATGTG		Eurofins Genomics GmbH

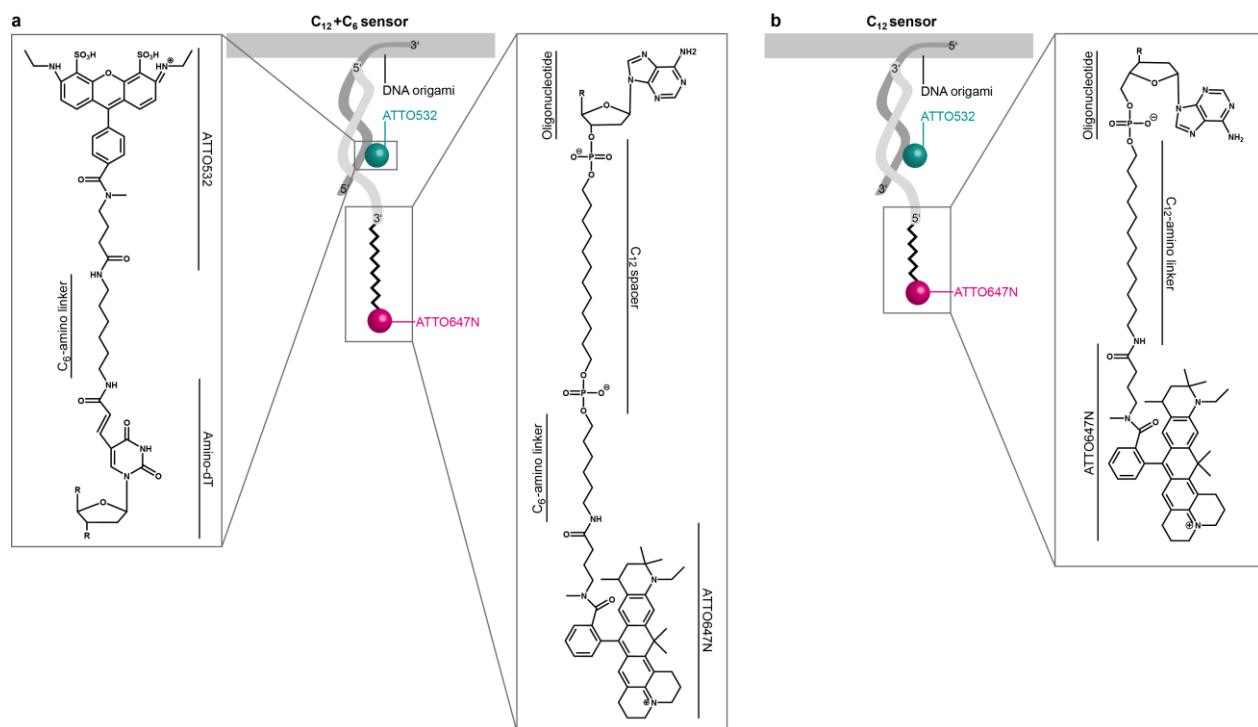


**Figure S2. Detailed sketch of the different voltage-sensor designs.** (a) For the  $C_{12}+C_6$  sensor, a strand from the DNA origami is extended from the 5' end (dark grey) and carries an ATTO532 (cyan, zoom-in left for details). In light grey, the counter strand is shown with the 3' end carrying a carbon chain and an ATTO647N (pink). The right zoom-in shows how the ATTO647N is connected to the DNA's 3' end via a  $C_{12}$  spacer and a  $C_6$ -amino linker. (b) For the  $C_{12}$  sensor, the strand in the origami is extended on the 3' end (dark grey) and also carries the ATTO532 (cyan) which is connected as shown in the zoom-in in (a). The counter strand carries on the 5' end the carbon chain with the ATTO647N. In the zoom-in, the connection between the 5' end of the DNA and the ATTO647N via a  $C_{12}$ -amino linker is shown.



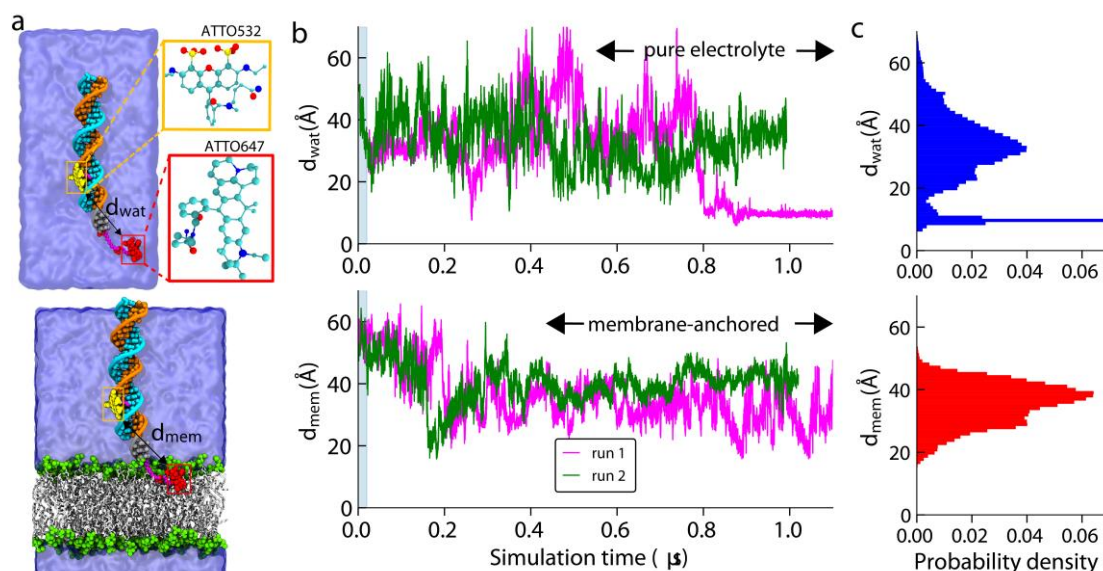


**Figure S3. Equilibrium MD simulation of dye conjugated dsDNA in aqueous and membrane anchored environment.** (a) A cut-away view of the all-atom models of 22-base pair long dsDNA conjugated to ATTO532 (yellow) and ATTO647N (red) dye molecules, solvated in the aqueous solution (top panel); anchored to lipid bilayer membrane and then solvated (bottom panel). The alkyl carbon chains ( $C_6$  and  $C_{12}$ ) connecting the dye molecules to the DNA (as shown in the chemical sketch in Figure S2) are shown in magenta. Complementary strands of the DNA are shown in turquoise and orange, the DOPC lipid head groups are shown as green spheres whereas the lipid tails are shown as white lines, water and ions are not shown for the sake of clarity. The enlarged atomic structures of the respective dye molecules are shown in yellow and red boxes. (b) Distance between the center of mass of the ATTO532 and ATTO647N dye molecules as a function of simulation time from two independent simulation runs in a box of water (top panel) and while anchored in lipid bilayer membrane (bottom panel). (c) The histogram of the distance between the dye molecules in water (top) and while anchored in membrane (bottom) excluding the first 200 ns from each simulation run.

**Table S2. Concentration of KCl and NaCl in the buffer inside and outside of the LUVs.** To build up a certain transmembrane potential  $\Delta\Psi$  with respect to the Nernst equation, the buffers used inside and outside of the LUVs were varied. The KCl gradient is responsible for the potential creation whereas NaCl is added to prevent osmotic pressure. The NaCl/KCl concentrations add up to buffers containing 5 mM Tris, 1 mM EDTA and 0.5 mM Trolox at pH 7 as previously described as the LUV buffer.

$\Delta\Psi$ [mV]	$c_{\text{inside}}$ [mM]		$c_{\text{outside}}$ [mM]	
	KCl	NaCl	KCl	NaCl
-125	150	0	1.1	148.9
-100	150	0	3	147
-75	150	0	8	142
-50	150	0	21	129
-25	150	0	56	94
0	150	0	150	0
0	1	149	1	149
25	1	149	2.7	147.3
50	1	149	7	143
75	1	149	19	131
100	1	149	50	100
125	1	149	134	16

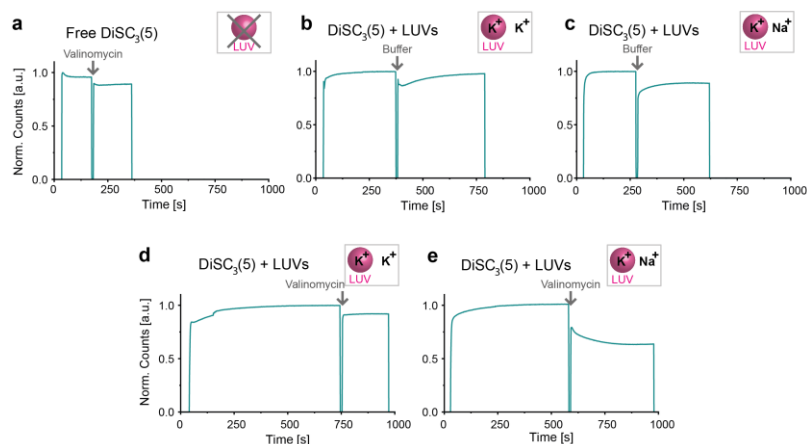


**Figure S4. Valinomycin bulk test.** On a spectrofluorometer, it was proven that a transmembrane potential  $\Delta\Psi$  is built up with the valinomycin assay using the voltage-sensitive dye DiSC<sub>3</sub>(5). As a control, the DiSC<sub>3</sub>(5) was investigated without LUVs in the cuvette and valinomycin was added to the solution (a). The intensity drop results from the dye sticking to the pipette tip while adding the solution. No further effect is observed. As another control, LUVs with potassium buffer inside and outside of the liposome (b) and inside potassium and outside sodium (c) were used and buffer was added to the samples. The intensity drop due to dye sticking to the pipette is observed as previously. Further, the intensity equilibrates after the buffer addition for both samples which is related to the homogeneous distribution after Brownian motion in the field of view. Next, valinomycin was added to LUVs with inside and outside potassium ions and buffer was injected (d). As for the other controls, an intensity drop due to dye sticking is observed, but no further effect. Only LUVs with inside potassium and outside sodium show a clear drop in intensity (e) which equilibrates after a while following Brownian motion. As more of the DiSC<sub>3</sub>(5) is attracted to the charged membrane, contact quenching of the dyes take place and the intensity is reduced. For details see the chapter on “Valinomycin bulk assay” above.

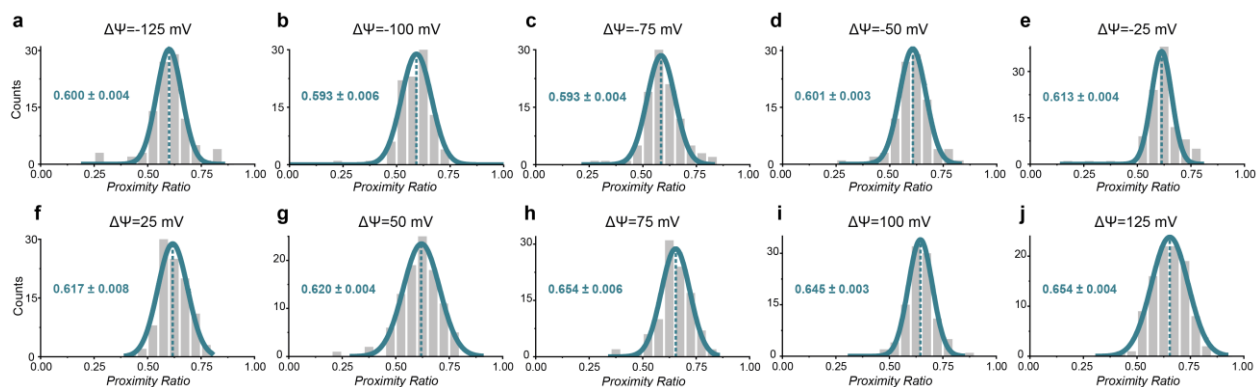


**Figure S5. PR distributions for all samples of the  $C_{12}+C_6$  sensor with transmembrane potentials  $\Delta\Psi$ .** The samples were imaged after buffer exchange, addition of valinomycin and hence, the creation of a transmembrane potential of (a)  $\Delta\Psi=-125$  mV, (b)  $\Delta\Psi=-100$  mV, (c)  $\Delta\Psi=-75$  mV, (d)  $\Delta\Psi=-50$  mV, (e)  $\Delta\Psi=-25$  mV, (f)  $\Delta\Psi=25$  mV, (g)  $\Delta\Psi=50$  mV, (h)  $\Delta\Psi=75$  mV, (i)  $\Delta\Psi=100$  mV and (j)  $\Delta\Psi=125$  mV. The respective mean resulting from the Gauss fit as well as the standard error of the mean is given for each distribution.  $N_{\text{molecule}}$ : (a)-(j) 100.

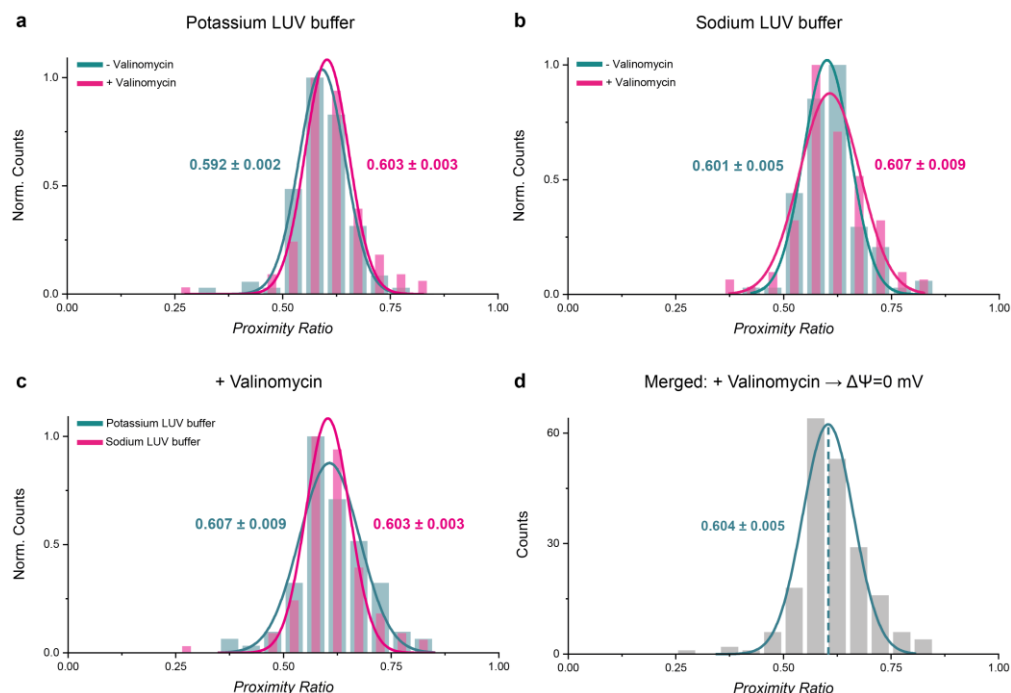


**Figure S6. PR distributions of various  $C_{12}+C_6$  samples compared.** Control for  $\Delta\Psi=0$  mV with potassium LUV buffer in cyan with the sample after the addition of valinomycin in pink (a), control for  $\Delta\Psi=0$  mV with sodium LUV buffer in cyan with the sample after the addition of valinomycin in pink (b) and both  $\Delta\Psi=0$  mV samples in potassium (cyan) and sodium (pink) LUV buffer with their respective mean from Gauss fitting and the standard error of the mean. All derived mean values are very similar which is why on the one hand a buffer effect on the PR value and on the other hand an effect of the valinomycin can be neglected. Therefore, the data for both samples with valinomycin (c) are merged and presented in (d) which in the following is the  $\Delta\Psi=0$  mV sample.  $N_{\text{molecule}}$ : (a)-(c) 100 for each distribution, (d) 200.

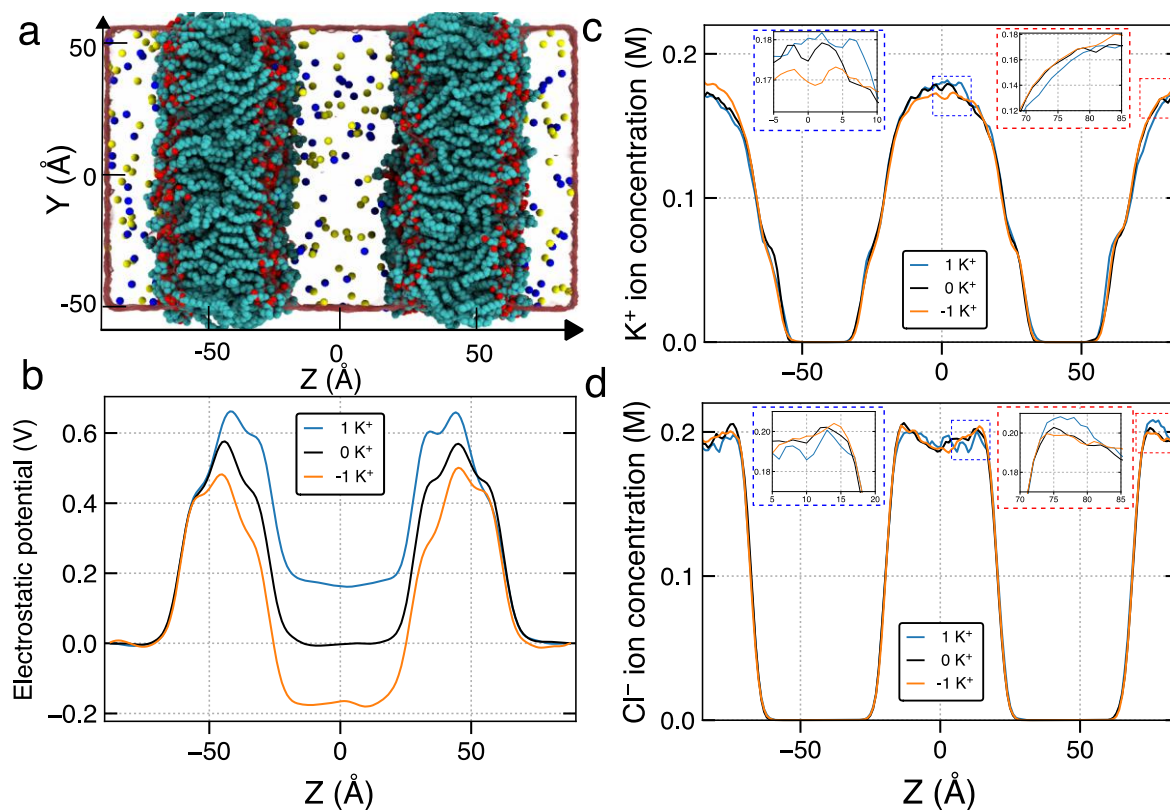


**Figure S7. Voltage bias created by shuffling of a single ion in double membrane systems.** (a) A representative snapshot of the all-atom model of double DOPC lipid bilayer membrane solvated in 150 mM solution of KCl. Non-hydrogen atoms of the lipid (DOPC) membrane are shown as blue (N), tan (P), red (O), and cyan (C) spheres. The transparent surface illustrates the volume occupied by the water molecules. The potassium and chloride ions are shown in blue and yellow spheres. (b) Average electrostatic potential profile of various systems along the z-axis. Local concentration of (c) potassium and (d) chloride ions along the lipid bilayer normal averaged over last 300 ns of NVT simulation. The images inside the close-in boxes shows the zoomed in region in the plots. The density was obtained by dividing the z-axis in the bins of 1 Å and then Savitzky Golay filter (window length 21 with a polynomial of degree 2) is used for smoothing of the data.

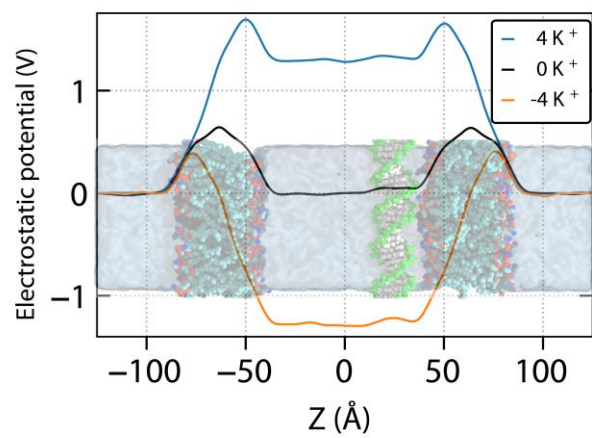


**Figure S8.** Average electrostatic profile of the 0 K<sup>+</sup>, 4 K<sup>+</sup> and -4 K<sup>+</sup> systems along the bilayer normal during the REUS MD simulations.

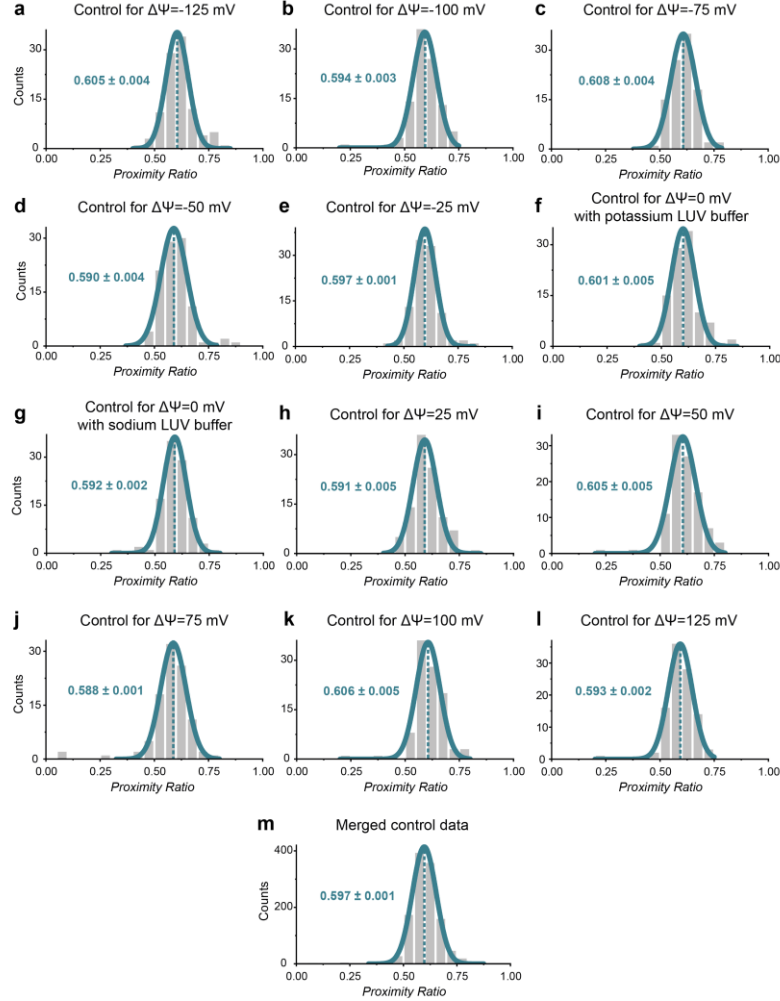


**Figure S9. PR distributions for all control samples of the  $C_{12}+C_6$  sensor.** The samples were imaged before buffer exchange and transmembrane potential creation via valinomycin and the plots show the distributions with their respective mean and standard error of the mean from the Gauss fit. Control sample resulting in (a)  $\Delta\Psi=-125$  mV, (b)  $\Delta\Psi=-100$  mV, (c)  $\Delta\Psi=-75$  mV, (d)  $\Delta\Psi=-50$  mV, (e)  $\Delta\Psi=-25$  mV, (f)  $\Delta\Psi=0$  mV with potassium LUV buffer, (g)  $\Delta\Psi=0$  mV with sodium LUV buffer, (h)  $\Delta\Psi=25$  mV, (i)  $\Delta\Psi=50$  mV, (j)  $\Delta\Psi=75$  mV, (k)  $\Delta\Psi=100$  mV, (l)  $\Delta\Psi=125$  mV. As all of the samples show similar mean values, their data is merged and plotted together in (m) and further referred to as the sample before the valinomycin addition.  $N_{\text{molecule}}$ : (a)-(l) 100, (m) 1200.



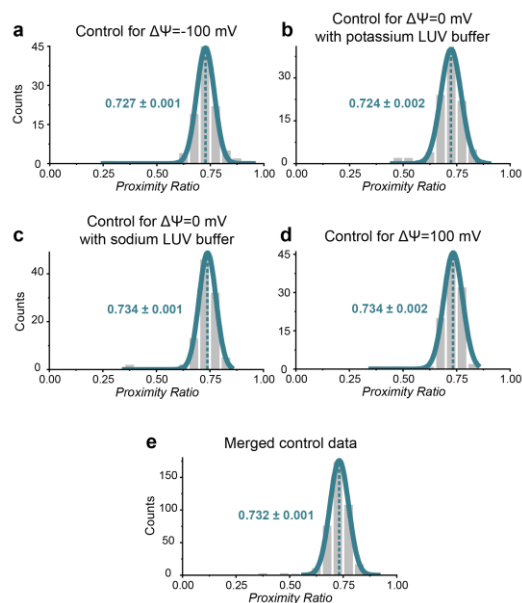


**Figure S10. PR distributions for all control samples of the C<sub>12</sub> sensor.** The samples were imaged before buffer exchange and transmembrane potential creation via valinomycin and the plots show the distributions with their respective mean and standard error of the mean from the Gauss fit. Control sample resulting in (a)  $\Delta\Psi = -100$  mV, (b)  $\Delta\Psi = 0$  mV with potassium LUV buffer, (c)  $\Delta\Psi = 0$  mV with sodium LUV buffer and (d)  $\Delta\Psi = 125$  mV. As all of the samples show similar mean values, their data is merged and plotted together in (e) and further referred to as the sample before the valinomycin addition.  $N_{\text{molecule}}$ : (a)-(d) 100, (e) 400.

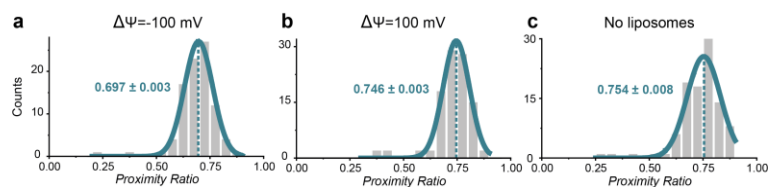


**Figure S11. PR distributions for samples of the  $C_{12}$  sensor with transmembrane potentials  $\Delta\Psi$  and without liposomes.** For the creation of transmembrane potentials of (a)  $\Delta\Psi = -100$  mV and (b)  $\Delta\Psi = 100$  mV, the outside buffer was exchanged and valinomycin was added to create the potentials. (c) PR distribution for sample without liposomes. The respective mean resulting from the Gauss fit as well as the standard error of the mean is given for each distribution.  $N_{\text{molecule}}$ : (a) 91, (b)-(c) 100.

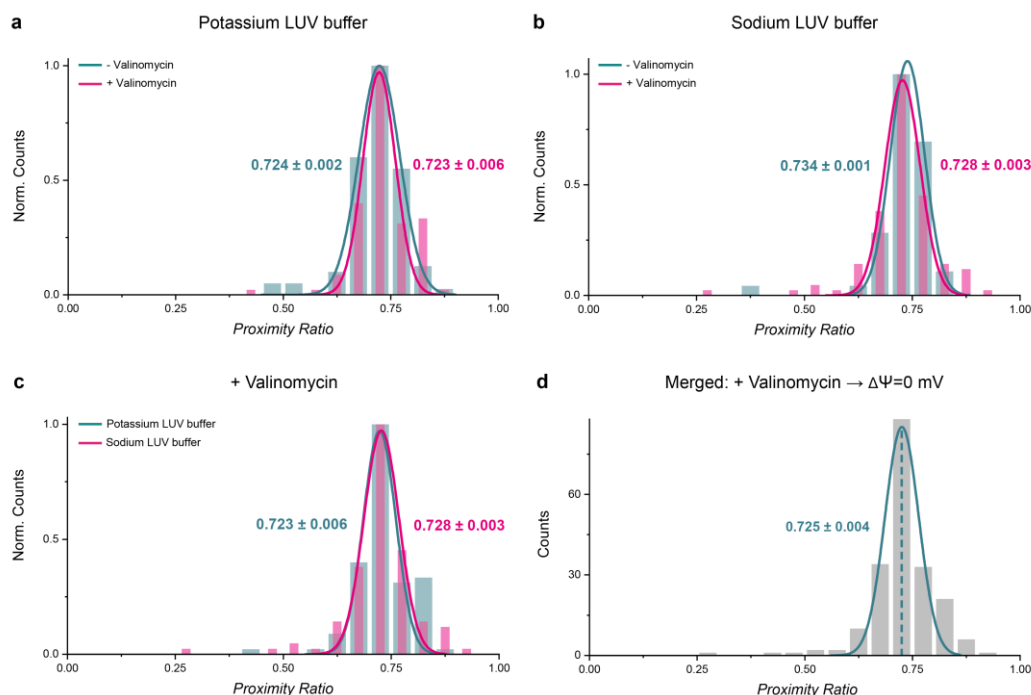
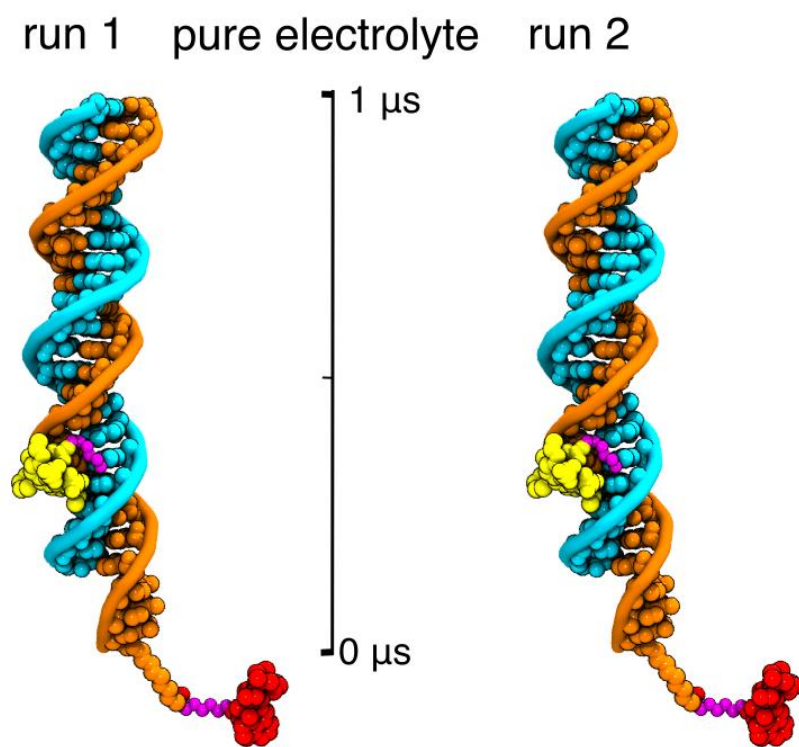
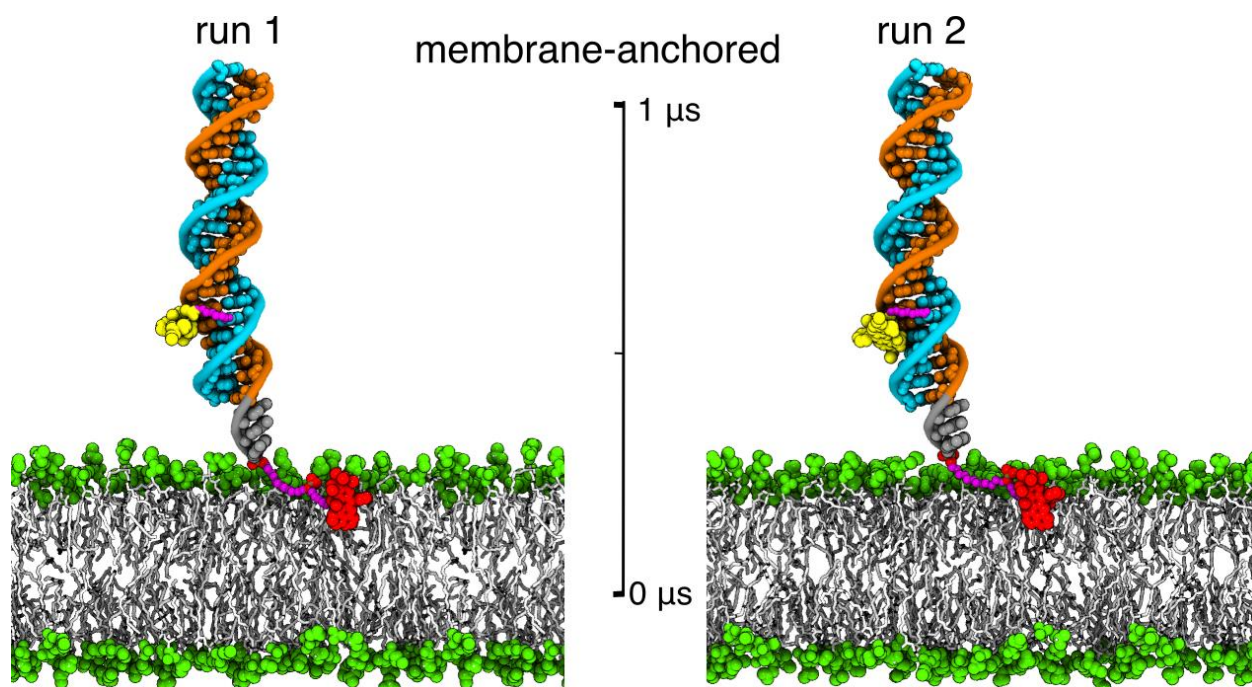


**Figure S12. PR distributions of various  $C_{12}$  samples compared.** Control for  $\Delta\Psi=0$  mV with potassium LUV buffer in cyan with the sample after the addition of valinomycin in pink (a), control for  $\Delta\Psi=0$  mV with sodium LUV buffer in cyan with the sample after the addition of valinomycin in pink (b) and both  $\Delta\Psi=0$  mV samples in potassium (cyan) and sodium (pink) LUV buffer with their respective mean from Gauss fitting and the standard error of the mean. All derived mean values are very similar which is why on the one hand a buffer effect on the PR and on the other hand an effect of the valinomycin can be neglected. Therefore, the data for both samples with valinomycin (c) are merged and presented in (d) which in the following is the  $\Delta\Psi=0$  mV sample.  $N_{\text{molecule}}$ : (a) cyan: 100, pink: 99, (b) each 100, (c) cyan: 99, pink: 100, (d) 199.

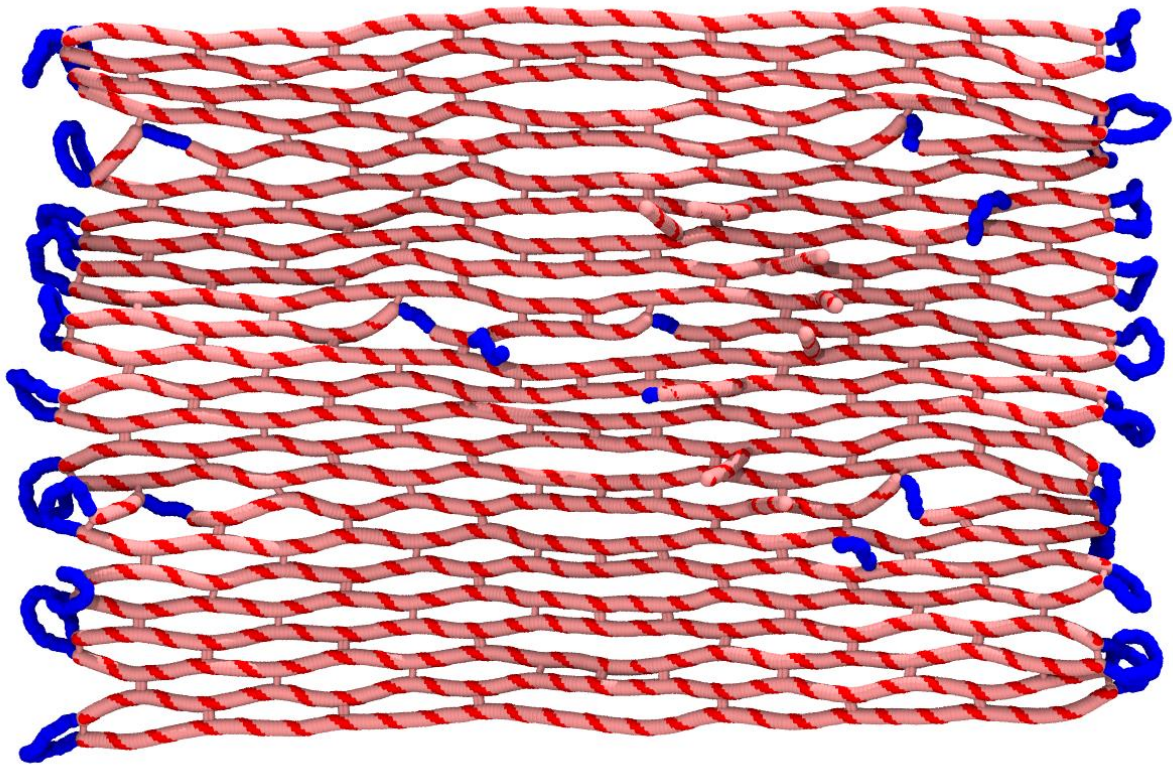
## Captions to Supplementary Movies



**Supplementary Movie 1.** All-atom molecular dynamics simulation of ATTO532 (yellow) and ATTO647N (red) dye molecules conjugated to dsDNA in purely aqueous solution. The movie illustrates MD trajectories of two independent simulation runs (run 1 and run 2) starting from the same initial configuration. Water and ions are not shown for clarity.



**Supplementary Movie 2.** All-atom molecular dynamics simulation of ATTO532 (yellow) and ATTO647N (red) dye molecules conjugated to dsDNA anchored in DOPC lipid bilayer membrane. The movie illustrates MD trajectories of two independent simulation runs (run 1 and run 2) starting from the same initial configuration. Water and ions are not shown for clarity.



**Supplementary Movie 3. A typical mrDNA<sup>18</sup> simulation of the DNA origami plate designed as a sensor of transmembrane potentials.** The coarse-grained simulation starts with the caDNAno design of the origami plate which is first mapped into a 5-bp/bead model followed by a 1-bead/bp model. Finally, the all-atom model of the system was obtained by averaging equilibrated conformations in coarse-grained simulation. At the end, the all-atom model was simulated for couple of nanoseconds in vacuum using the network of elastic restraints.<sup>29</sup>

## References

- (1) Schmied, J. J.; Gietl, A.; Holzmeister, P.; Forthmann, C.; Steinhauer, C.; Dammeyer, T.; Tinnefeld, P. Fluorescence and super-resolution standards based on DNA origami. *Nature methods* **2012**, *9*, 1133–1134.
- (2) Douglas, S. M.; Marblestone, A. H.; Teerapittayanon, S.; Vazquez, A.; Church, G. M.; Shih, W. M. Rapid prototyping of 3D DNA-origami shapes with caDNAno. *Nucleic acids research* **2009**, *37*, 5001–5006.
- (3) Hope, M. J.; Bally, M. B.; Webb, G.; Cullis, P. R. Production of large unilamellar vesicles by a rapid extrusion procedure. Characterization of size distribution, trapped volume and ability to maintain a membrane potential. *Biochimica et Biophysica Acta (BBA) - Biomembranes* **1985**, *812*, 55–65.
- (4) Preus, S.; Noer, S. L.; Hildebrandt, L. L.; Gudnason, D.; Birkedal, V. iSMS: Single-molecule FRET microscopy software. *Nat Methods* **2015**, *12*, 593–594.
- (5) Phillips, J. C.; Hardy, D. J.; Maia, J. D. C.; Stone, J. E.; Ribeiro, J. V.; Bernardi, R. C.; Buch, R.; Fiorin, G.; Hénin, J.; Jiang, W.; et al. Scalable molecular dynamics on CPU and GPU architectures with NAMD. *The Journal of chemical physics* **2020**, *153*, 44130.
- (6) Batcho, P. F.; Case, D. A.; Schlick, T. Optimized particle-mesh Ewald/multiple-time step integration for molecular dynamics simulations. *The Journal of chemical physics* **2001**, *115*, 4003–4018.
- (7) Feller, S. E.; Zhang, Y.; Pastor, R. W.; Brooks, B. R. Constant pressure molecular dynamics simulation: The Langevin piston method. *The Journal of chemical physics* **1995**, *103*, 4613–4621.
- (8) Miyamoto, S.; Kollman, P. A. Settle: An analytical version of the SHAKE and RATTLE algorithm for rigid water models. *J. Comput. Chem.* **1992**, *13*, 952–962.
- (9) Andersen, H. C. Rattle: A “velocity” version of the shake algorithm for molecular dynamics calculations. *Journal of Computational Physics* **1983**, *52*, 24–34.
- (10) Hart, K.; Foloppe, N.; Baker, C. M.; Denning, E. J.; Nilsson, L.; Mackerell, A. D. Optimization of the CHARMM additive force field for DNA: Improved treatment of the BI/BII conformational equilibrium. *Journal of chemical theory and computation* **2012**, *8*, 348–362.
- (11) Klauda, J. B.; Venable, R. M.; Freites, J. A.; O'Connor, J. W.; Tobias, D. J.; Mondragon-Ramirez, C.; Vorobyov, I.; Mackerell, A. D.; Pastor, R. W. Update of the CHARMM all-atom additive force field for lipids: validation on six lipid types. *The journal of physical chemistry. B* **2010**, *114*, 7830–7843.
- (12) Beglov, D.; Roux, B. Finite representation of an infinite bulk system: Solvent boundary potential for computer simulations. *The Journal of chemical physics* **1994**, *100*, 9050–9063.
- (13) Yoo, J.; Aksimentiev, A. Improved Parametrization of Li<sup>+</sup>, Na<sup>+</sup>, K<sup>+</sup>, and Mg<sup>2+</sup> Ions for All-Atom Molecular Dynamics Simulations of Nucleic Acid Systems. *J. Phys. Chem. Lett.* **2012**, *3*, 45–50.
- (14) Yoo, J.; Aksimentiev, A. Improved Parameterization of Amine-Carboxylate and Amine-Phosphate Interactions for Molecular Dynamics Simulations Using the CHARMM and AMBER Force Fields. *Journal of chemical theory and computation* **2016**, *12*, 430–443.
- (15) Vanommeslaeghe, K.; Hatcher, E.; Acharya, C.; Kundu, S.; Zhong, S.; Shim, J.; Darian, E.; Guvench, O.; Lopes, P.; Vorobyov, I.; et al. CHARMM general force field: A force field for drug-like molecules compatible with the CHARMM all-atom additive biological force fields. *J. Comput. Chem.* **2010**, *31*, 671–690.
- (16) Humphrey, W.; Dalke, A.; Schulten, K. VMD: Visual molecular dynamics. *Journal of Molecular Graphics* **1996**, *14*, 33–38.
- (17) Case, D. A.; V. Babin; J.T. Berryman; R.M. Betz; Q. Cai; D.S. Cerutti; T.E. Cheatham, I.; T.A. Darden; R.E. Duke; H. Gohlke; et al. *AMBER 14*; San Francisco, 2014.



- (18) Maffeo, C.; Aksimentiev, A. MrDNA: a multi-resolution model for predicting the structure and dynamics of DNA systems. *Nucleic acids research* **2020**, *48*, 5135–5146.
- (19) Vanommeslaeghe, K.; Mackerell, A. D. Automation of the CHARMM General Force Field (CGenFF) I: bond perception and atom typing. *Journal of chemical information and modeling* **2012**, *52*, 3144–3154.
- (20) Jorgensen, W. L.; Chandrasekhar, J.; Madura, J. D.; Impey, R. W.; Klein, M. L. Comparison of simple potential functions for simulating liquid water. *The Journal of chemical physics* **1983**, *79*, 926–935.
- (21) Jo, S.; Kim, T.; Iyer, V. G.; Im, W. CHARMM-GUI: a web-based graphical user interface for CHARMM. *J. Comput. Chem.* **2008**, *29*, 1859–1865.
- (22) Schröder, T.; Scheible, M. B.; Steiner, F.; Vogelsang, J.; Tinnefeld, P. Interchromophoric Interactions Determine the Maximum Brightness Density in DNA Origami Structures. *Nano letters* **2019**, *19*, 1275–1281.
- (23) Di Fiori, N.; Meller, A. The Effect of dye-dye interactions on the spatial resolution of single-molecule FRET measurements in nucleic acids. *Biophysical journal* **2010**, *98*, 2265–2272.
- (24) Minhas, V.; Sun, T.; Mirzoev, A.; Korolev, N.; Lyubartsev, A. P.; Nordenskiöld, L. Modeling DNA Flexibility: Comparison of Force Fields from Atomistic to Multiscale Levels. *The journal of physical chemistry. B* **2020**, *124*, 38–49.
- (25) Morzy, D.; Rubio-Sánchez, R.; Joshi, H.; Aksimentiev, A.; Di Michele, L.; Keyser, U. F. Cations Regulate Membrane Attachment and Functionality of DNA Nanostructures. *Journal of the American Chemical Society* [Online early access]. DOI: 10.1021/jacs.1c00166. Published Online: May. 7, 2021.
- (26) Sugita, Y.; Kitao, A.; Okamoto, Y. Multidimensional replica-exchange method for free-energy calculations. *The Journal of chemical physics* **2000**, *113*, 6042–6051.
- (27) Fiorin, G.; Klein, M. L.; Hénin, J. Using collective variables to drive molecular dynamics simulations. *Molecular Physics* **2013**, *111*, 3345–3362.
- (28) Kumar, S.; Rosenberg, J. M.; Bouzida, D.; Swendsen, R. H.; Kollman, P. A. THE weighted histogram analysis method for free-energy calculations on biomolecules. I. The method. *J. Comput. Chem.* **1992**, *13*, 1011–1021.
- (29) Maffeo, C.; Yoo, J.; Aksimentiev, A. De novo reconstruction of DNA origami structures through atomistic molecular dynamics simulation. *Nucleic acids research* **2016**, *44*, 3013–3019.